NMR IN BIOMEDICINE, VOL. **10**, 394–410 (1997)

Theory and Application of Array Coils in MR Spectroscopy

Steven M. Wright⋆ and Lawrence L. Wald†

Departments of Electrical Engineering and Radiology, Texas A&M University, College Station TX, USA and † Brain Imaging Center, McLean Hospital and Consolidated Department of Psychiatry, Harvard Medical School, Belmont, MA, USA

The theory and application of array coils are reviewed in the context of phased array spectroscopy. The optimization of the signal-to-noise ratio from an array of coils is developed by considering the efficiency of a phased array transmit coil. This approach avoids the need to consider noise correlation, and should be useful in future considerations of transmit phased array coils for MR spectroscopy. Methods to characterize array coil performance, including fields and coupling are briefly summarized, along with methods to minimize the effects of mutual inductance. The signal-to-noise advantages of array coils over single coils are examined for both planar and cylindrical arrays. Numerical simulations of planar arrays of 2×2, 4×4 and 8×8 elements and constant overall dimension are compared to a single coil of the same size. The results demonstrate a significant improvement in sensitivity near the array coil. Although the benefits of the array decrease as a function of distance from the array, the array sensitivity never drops below that of a single coil with the same overall dimensions, or that of a single element of the array. Similar results are obtained for a sixteen element cylindrical array, which is compared to a standard quadrature birdcage coil using both computational methods and phantom measurements. The phased array techniques reviewed are demonstrated with proton spectroscopic images of the brain.

NMR Biomed. **10**, 394–410 (1997) No. of Figures: 17 No. of Tables: 1 No. of References: 89

Keywords: CSI; spectroscopic imaging; RF coils; phased arrays; SNR

Received 4 August 1997; accepted 25 August 1997

INTRODUCTION

Surface coil arrays were first implemented in MR imaging as switched coils, allowing different coils or combinations of coils to be used for different slices.[1–4] Examples include multislice axial imaging of the spine and sagittal imaging of the temporomandibular joints. Although a single coil can be optimized for a given observation point,[5] optimizing for large or multiple volumes without significantly sacrificing signal-to-noise ratio (SNR) requires multiple coils. Hyde[1] proposed using multiple receivers to independently and simultaneously obtain signals from multiple coils, achieving improved SNR from multiple regions with no increase in time. Roemer implemented a system using four receiver coils and four receiver channels, calling it an NMR phased array.[6] Additionally, Roemer described methods for combining the data from the multiple receivers to optimize the SNR in every voxel.

Over the last few years significant effort has gone into the development and application of array coils in MR imaging.[6–31] More recently several groups have domonstrated the potential for array coils and multiple channel receivers in MRS.[10, 25, 32, 33] This paper will review the theory, implementation and application of array coils in MRS. The general theory of the array coil will be developed from the context of a phased array transmit coil, rather than a receiver coil as initially described in detail by Roemer.[6] This approach was chosen because it avoids the issue of noise correlation, which has been the subject of some discussion.[6, 34–39] Additionally, this approach should be more applicable to the development of transmit array coils, a logical extension of array coil technology. Section III provides a summary of some of the details helpful in implementing array coils. For completeness, quasistatic methods for calculating flux maps and coil self and mutual-impedances are included. Additionally, methods for measuring and minimizing the coupling between antennas are briefly discussed. Section IV includes several examples of the application of array coils in chemical shift imaging, along with new theoretical and phantom results demonstrating the SNR gain obtained by planar and cylindrical array coils.

THEORY AND IMPLEMENTATION OF PHASED ARRAYS FOR NMR SPECTROSCOPY

A generalized phased array receiving antenna is illustrated in Fig. 1(a). In order to optimize the signal-to-noise ratio obtained from the chosen observation point, the relative amplitudes and phases of the signals from each element are adjusted before combining. The relative amplitudes and phases form a set of complex weighting coefficients [w], where $w_i=|w_i|e^{j\phi_i}$. When multiple receiver channels are available, as in MRI/MRS applications, it is of great advantage to simply record the N independent signals and

⋆ Correspondence to: S. M. Wright.

Contract grant sponsor: National Science Foundation; *contract grant number:* BCS-9308921.

Abbreviations used: NAN, N-acetyl aspartate; RF, Radio-frequency; S/m, Siemens per meter; SNR, Signal-to-noise ratio; Z-parameters, impedance parameters; S-parameters; scattering parameters.

 CCC 0952–3480/97/080394–17 $17.50

process the data retrospectively. In this way the data can be processed in different ways to realize different objectives. For example, one may wish to minimize the contribution from one area, or, alternatively, to maximize the signal-to-noise ratio at another, or even perform a combination of both. The signals are independently demodulated and digitized, using either multiple receiver channels[6, 28] or time-domain multiplexing.[40–42]

The general problem at hand is to determine the set of weighting functions [w] that optimize the signal-to-noise ratio obtained from the array. These weighting functions will be different for each voxel in the image or spectroscopic image. For conceptual purposes, it is convenient to invoke reciprocity[43, 44] and consider the equivalent problem of determining the element currents that maximize the coil efficiency, η_c, at the location of interest. While reciprocity was introduced to the NMR literature for the analysis of a single coil,[44] it applies equally well to arrays of coils, and is commonly used for the analysis of arrays in the antenna literature.[45] The coil efficiency as a transmitter is defined as the ratio of the effective power density produced at the voxel of interest to the total power absorbed by the array. This transforms the problem to one of optimizing the transmit phased array of Fig. 1(b). However, unlike the optimization of a true transmit array where the gain and phase changes necessarily effect all voxels, the optimization of the receive-array will be applied in post-processing to each voxel in the image or spectroscopic image.

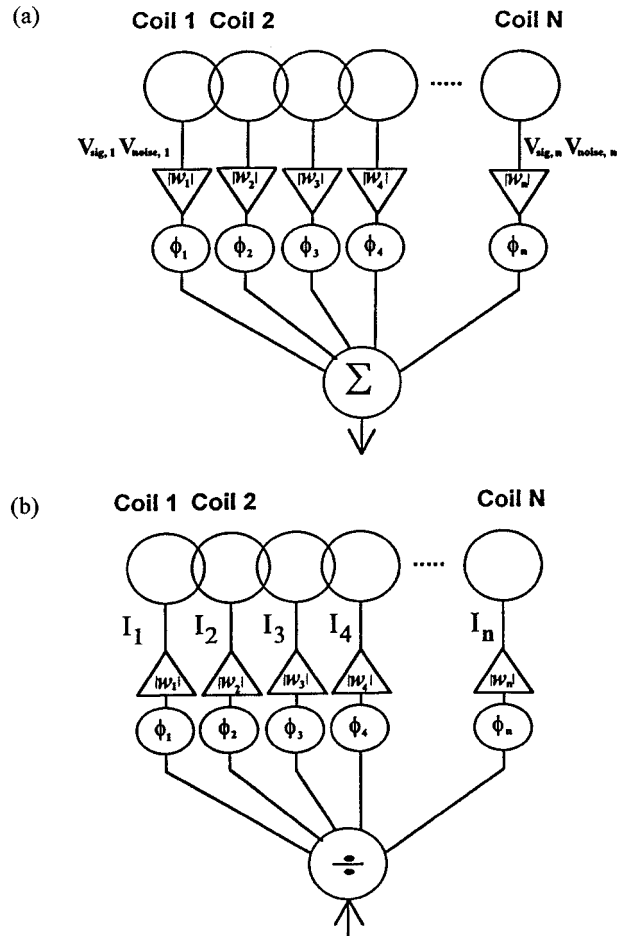

Figure 1. (a) Block diagram of a phased array receiver coil. The weighting coefficients $w_i=|W_i|e^{j\phi_i}$ are chosen to optimize the signal-to-noise ratio from each voxel. (b) Block diagram of a phased array transmitter coil. The weighting coefficients $w_i=|W_i|e^{j\phi_i}$ are chosen to optimize the ratio of transmitted power to absorbed power for each voxel. This optimises the coil 'efficiency', and is equivalent to optimizing the signal-to-noise ratio in the receiver case, resulting in the same weighting coefficients. Note that the current entering each phase shifter is the same, and can be assumed to be 1 amp, giving $I_i=w_i$.

SNR and coil efficiency for a single coil

In the MR literature, the SNR is usually defined as the ratio of the signal voltage to the noise voltage. Immediately following a 90° pulse the signal voltage can be shown to be:

$$V_{sig}=\sqrt{2}\omega_o\Delta V M_o \mathbf{B}_1\cdot\hat{\mathbf{p}} \quad (1)$$

where ω_o is the Larmor frequency in rad/sec, ΔV is the volume of interest, M_o is the magnetization, $\mathbf{B}_1$ is the field produced by the coil with 1 amp of current, and $\hat{\mathbf{p}}$ is one of two circularly polarized unit vectors $\hat{\mathbf{p}}=(\hat{a}_x\pm j\hat{a}_y)/\sqrt{2}$, chosen based on the sign convention used and the direction of the static magnetic field. We can denote B_t to be the effective transverse magnetic field (again with one amp of current at the coil terminals),

$$B_t=|B_t|e^{j\theta}=\vec{B}_1\cdot\hat{}p \quad (1)$$

where θ is the phase of the field relative to an arbitrary phase reference.

The noise voltage, V_{noise}, produced by a coil with impedance $Z_{coil}=R_{coil}+jX_{coil}$ is given by

$$V_{noise}=\sqrt{4kT\Delta f R_{coil}} \quad (3)$$

The ratio of these two voltages gives the voltage signal to noise, SNR_v:

$$SNR_v=\frac{|V_{sig}|}{V_{noise}}=\frac{\sqrt{2}\omega_o\Delta V M_o|B_t|}{\sqrt{4kT\Delta f R}} \quad (4)$$

For purposes of this analysis, the constants which remain unchanged from voxel to voxel can be ignored, giving a 'coil signal-to-noise ratio' SNR_c:

$$SNR_c=\frac{\sqrt{2}|B_t|}{\sqrt{R}} \quad (5)$$

Equation (5) describes the voltage SNR of a receive coil in terms of the flux density it would produce as a transmit coil. The transmit coil efficiency, is, or course closely related to this expression. One can define the 'coil efficiency' as the ratio of the effective power density delivered to the observation point to the total power absorbed by the coil, P_{abs}. Noting that only the transverse power density is of importance in MRI and MRS, and once again ignoring fixed constants, the coil efficiency can be defined:

$$\eta_c=\frac{|B_t|^2}{P_{abs}}=\frac{B_t^* B_t}{\frac{1}{2}|I|^2 R} \quad (6)$$

Finally, noting that by the definition of B_t, $|I|=1$ Amp, Eqs (5) and (6) provide the link between the coil efficiency as a transmitter and the signal-to-noise ratio it produces as a receiver:

$$\eta_c=SNR_c^2=\frac{|B_t|^2}{P_{abs}} \quad (7)$$

This is particularly useful in comparing array coils.

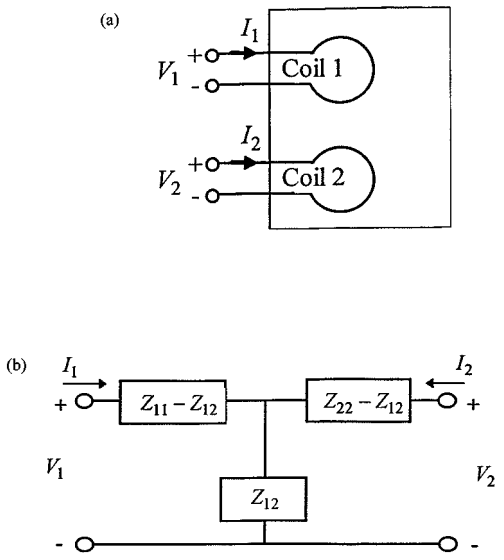

Figure 2. (a) Two array elements represented as a two-port circuit defined by the port voltages and currents. (b) 'T' equivalent representation of the two-port circuit in (a). The port voltage and current relationships are defined by the port open-circuit impedance parameters.

SNR of coil arrays

Consider an array of two coils, forming a simple two port network illustrated in Fig. 2(a). Any two port (or N-port) can be characterized by the terminal voltages and currents, V_i and I_j, and their ratios, known as the port open-circuit impedance elements, Z_{ij}.[43, 45] Z_{ij} is the ratio of the voltage at port i to the current at port j, with all other ports open circuited:

$$Z_{ij}=\left.\frac{V_i}{I_j}\right|_{I_k=0,\ k\neq j} \tag{8}$$

The port open-circuit impedance parameters can easily be measured using a network analyzer such as the HP4195a or a vector impedance meter such as the HP4193a (Hewlett-Packard, Palo-Alto, CA). For a two-port network, the network equations are:

$$\begin{aligned} V_1&=I_1Z_{11}+I_2Z_{12}\\ V_2&=I_1Z_{21}+I_2Z_{22}\end{aligned} \tag{9}$$

The coupling between ports, or coils, is defined by the mutual impedance Z_{12} and Z_{21}. By reciprocity, one can show that $Z_{12}=Z_{21}$.[43]

The network equations in Eq. (9) lead to a 'T' equivalent circuit representation of the two element coil array, shown in Fig. 2(b). One can easily compute the real power dissipated in this two-port network as:

$$P_{abs}=\tfrac{1}{2}(|I_1|^2R_{11}+|I_2|^2R_{22}+2(I_1^*I_2+I_2^*I_1)R_{12}) \tag{10}$$

which, for convenience in what follows, can be expressed as:

$$P_{abs}=\tfrac{1}{2}[I^*]^T[R][I] \tag{11}$$

where $[R]$ is the matrix comprised of the real components of the impedance matrix $[Z]$, with elements Z_{ij}. [I] is a column matrix representing the currents in each element of the array, and $[I^*]^T$ is a row matrix given by the conjugate-transpose of [I]:

$$[I]=\begin{bmatrix} I_1\\ I_2\\ \vdots\\ I_N\end{bmatrix}\quad [R]=\begin{bmatrix} R_{11} & R_{12} & \cdots & R_{1N}\\ R_{21} & R_{22} & & \\ \vdots & & \ddots & \\ R_{N1} & & & R_{NN}\end{bmatrix}$$

$$[I^*]^T=[\,I_1^* \quad I^* \quad \ldots \quad I_N^*\,] \tag{12}$$

The effective flux density produced at the observation point by the array, $B_{t,\,array}$, is a simple summation of B_t of each coil with 1 amp, weighted by the current into each coil:

$$B_{t,\,array}=\sum_{i=1}^{N_{coils}} I_iB_{ti}=[I]^T[B_t] \tag{13}$$

In order to obtain the coil efficiency given in Eq. (7), one needs $|B_{t,\,array}|^2$:

$$|B_{t,\,array}|^2=B^*_{t,\,array}\,B_{t,\,array}=[I^*]^T[B_t^*]\,[B_t]^T[I] \tag{14}$$

Equations [11] and [14] gives the effective flux density and the power absorbed by the array. Substitution into Eq. (7) obtains the efficiency of a coil array, or equivalently, the square of the array SNR:

$$\eta_c=\frac{[I^*]^T[B_t^*]\,[B_t]^T[I]}{\frac{1}{2}[I^*]^T[R]\,[I]} \tag{15}$$

Equation (15) is a ratio of quadratic Hermitian forms, one that commonly arises in optimization problems.[46, 47] In the next section the set of currents which optimizes η_c are determined.

Optimization of array signal-to-noise ratio

The current matrix $[I]$ which optimizes η_c can be obtained by taking the partial derivatives with respect to either the currents or their conjugate. This is done by writing the quadratic forms as double sums and taking the derivatives explicitly.

$$\eta_c=\frac{\displaystyle\sum_{i=1}^{N} I_i^*B_{ti}^*\sum_{j=1}^{N} B_{ti}I_i}{\displaystyle\frac{1}{2}\sum_{i=1}^{N}\sum_{j=1}^{N} I_i^*R_{ij}I_j} \tag{16}$$

Taking the derivative with respect to each of I_i^* leads to the set of N equations:

$$\frac{\partial\eta_c}{\partial I_i^*}=\frac{1}{P_{abs}^2}\left[P_{abs}\sum_j B_{ij}^*B_{ti}I_i-|B_t|^2\sum_j R_{ij}I_j\right]\quad i=1,N \tag{17}$$

Setting each equation to zero and writing the equations in matrix form gives:

$$[B_t^*]\,[B_t]^T[I]=\eta_c[R]\,[I] \tag{18}$$

Substituting for η_c from Eq. (15) above, one obtains

$$[B_t^*]\,[B_t]^T[I]=\frac{[I^*]^T[B_t^*]\,[B_t]^T[I]}{\frac{1}{2}[I^*]^T[R]\,[I]}\,[R]\,[I] \tag{19}$$

which can be simplified to:

$$[B_t^*]=\left\{\frac{[I^*]^T[B_t^*]}{\frac{1}{2}[I^*]^T[R][I]}\right\}[R][I] \quad (20)$$

The term in the braces reduce to a scalar, which will be denoted as $1/\lambda$. Thus, we have an expression which can be solved for the optimal current vector:

$$[B_t^*]=\frac{1}{\lambda}[R][I] \quad (21)$$

The excitation currents needed for optimal antenna efficiency, or signal-to-noise ratio are:

$$[I]=\lambda[R]^{-1}[B_t^*] \quad (22)$$

The scalar λ does not affect the SNR, as it is applied to each current element. However, it can be chosen to maintain constant absorbed power for all observation points, or alternatively to maintain a constant effective flux density at all observation points. The former is achieved by substituting the current vector given by Eq. (22) into Eq. (11) and solving for constant absorbed power by differentiating the expression and setting the result to zero. This results in:

$$\lambda_{noise}=\{[B_t]^T[R]^{-1}[B_t^*]\}^{-1/2} \quad (23)$$

which is denoted λ_{noise} because it forces the denominator of the signal-to-noise expression to be constant from voxel-to-voxel. The effective flux-density, or the signal in the receiving case, can be held constant by similarly solving for λ that forces Eq. (14) to be constant, giving:

$$\lambda_{signal}=\{[B_t]^T[R]^{-1}[B_t^*]\}^{-1} \quad (24)$$

Signal combination for optimal SNR

The discussion above determined the current vector which optimized the transmit coil efficiency (the ratio of effective transverse flux density produced by the array to the power absorbed by the array). In a practical implementation of a transmit array these currents would be achieved using amplifiers and phase shifters which control the gain and phase shift in transmission networks leading to each antenna element. The gain and phase shift applied to each element is a weighting factor for that element, w_i, where $w_i=|w_i|e^{j\phi_i}$. Thus, the antenna current vector becomes $[I]=[w]^T[I_{in}]$, with $[w]^T=[w_1, w_2, \ldots, w_N]$. Without loss of generality one can assume that the input to each of the amplifiers is 1 amp, so that $[I]=[w]$.

As discussed above, and easily shown by reciprocity, optimizing the efficiency of a transmit array is equivalent to optimizing the SNR of a receiving array. In the receiving case $[w]$ are the weighting factors applied to the signals from the individual elements prior to summing them, as illustrated in Fig. 1(a). In the case of an NMR phased array, the signals from each element are demodulated by multiple receivers or a multiplexed receiver, and the weighting factors are calculated for each voxel in the dataset during post-processing. Once the weighting factors are determined, the individual spectra from different coils can be combined into a single SNR optimized spectra by simply summing the weighted spectra on a point-by-point basis:

$$S_{km}^c=\sum_{j=1}^{N} w_{jk}S_{jkm}=[w_k]^T[S_{km}] \quad (25)$$

where S_{km}^c is the combined spectra and S_{jkm} is the mth spectral point in the kth spectra from coil j. For chemical-shift imaging, k would run from 1 to N_{voxels}, the number of voxels. Otherwise, $k=1$. Equation [25] applies to the case where the voxel is small relative to the rate of variation of the flux density of individual coils. In this case, it is clear that the weighting functions derived are common to all spectral points. If the spectra are non-localized, the situation is not as clear. In principle, each spectral point can be optimized independently for highest SNR, but this would effect the validity of peak height information.

Assuming that the flux-density of each coil element is known (magnitude and phase), along with the self- and mutal resistances of the coils, the weighting functions are obtained from Eq. (22) with $[I]=[w]$, and the signal-to-noise ratio is obtained from Eq. (15). This is the most general case of signal combination, and is summarized in Table 1. Two simplifications are considered briefly below, and are also summarized in Table 1.

Zero mutual resistance. Clearly optimization of the combined spectra using the most general approach requires considerable information, using both the complex field maps and the coil resistive coupling matrix. Calculated field maps or maps obtained from a phantom may not be sufficiently accurate for signal combination with different samples. Similarly, $[R]$ is certainly load dependent. Thus, it may be necessary to measure the field maps and coupling matrix for each study. In either case, there is some question as to whether there would be sufficient improvement in SNR to justify this additional effort. Roemer has calculated that simply ignoring the effect of the mutual resistance, essentially equivalent to ignoring noise correlations, will lead to at worst an 11% decrease in SNR.[6] For these reasons, the studies that have appeared in the literature to date have all ignored the mutual resistance matrix. Additionally, if the coils are all matched to 50 ohms at the reference ports, then $[R]$ is simply 50 ohms times the identity matrix. The constant can be absorbed into the scaling constant, and $[R]$ simply drops out, giving:

$$[w_k]=\lambda_k[B_{tk}^*] \quad (26)$$

Substituting Eq. (23) or (24) into this expression gives the weighting function for noise normalized spectra:

$$[w_{k,\,noise}]=\frac{[B_{tk}^*]}{\sqrt{[B_{tk}]^T[B_{tk}^*]}}=\frac{[B_{tk}^*]}{\|B_{tk}\|} \quad (27)$$

Table 1. Summary of weighting functions and scaling constants for different combination methods

	General	Zero mutual resistance	SNR weighting
Additional data needed	Field maps, resistance matrix	Field maps	None
$[w]$	$\lambda[R]^{-1}[B_t^*]$	$\lambda[B_t^*]$	$\lambda[S_{km_{ref}}]$
λ_{noise}	$\{[B_t]^T[R]^{-1}[B_t^*]\}^{-1}$	$\|B_t\|^{-1}$	$\|S_{km_{ref}}\|^{-1}$

The combined spectra are obtained using Eq. (25), and the combined SNR is calculated using Eq. (15), with $[w]=[I]$. For constant sensitivity combination in CSI, the scaling constant λ is squared.

SNR weighting and the sum-of-squares approximation. A further simplification uses the signal intensity of each voxel as that voxel's weighting function. In spectroscopy, the relative heights of a particular spectral peak, or a linear combination of two or more peaks, can be used as an approximation to the flux density magnitudes at the location of the voxel from each coil. The weighting functions obtained for a voxel are then applied to each spectral point. Assuming that the spectra from each receiver are individually phased, and denoting the reference peak spectral point as m_{ref}, the weighting functions for the jth coil and the kth voxel become:

$$[w_{k,\,noise}]=\frac{[S_{km_{ref}}]}{\|S_{km_{ref}}\|} \tag{28}$$

Using Eq. (25) and simplifying, one obtains the equation for SNR weighted spectra:

$$S^c_{km}=\frac{[S_{km_{ref}}]^T[S_{km}]}{\|S_{km_{ref}}\|}=\frac{\sum_{j=1}^{N_{coils}}(S_{jkm_{ref}}S_{jkm})}{\sqrt{\sum_{j=1}^{N_{coils}}(S_{jkm_{ref}})^2}} \tag{29}$$

Equation (29) has been applied in several studies.[10, 25, 32, 33]

A final simplification can be made if one is combining a single set of images rather than spectral data. In this case the reference value for each pixel is simply the pixel itself, i.e., $S_{jkm_{ref}}=S_{jkm}$, since only one spectral point is being considered and $m=1$. Eq. (29) reduces to the sum-of-squares formula suggested by Roemer[6]

$$S^c_k=\sqrt{\sum_{j=1}^{N_{coils}}(s_{jk})^2} \tag{30}$$

MODELING AND IMPLEMENTATION OF PHASED ARRAY COILS

The information required to design, build and apply an array coil in MRS depends greatly on the application and the signal combination method to be used. At a minimum some knowledge of the self-impedances of the coils is needed to design matching networks. In designing the array, one would like to have maps of the flux densities produced by the coils and their mutual impedances. The determination of these quantities has and is being discussed in the literature, and a full discussion would exceed the scope of this paper. However, it is possible to minimize the effects of mutual coupling through some simple coil designs, and to model the mutual resistances and flux densities using simple static and quasistatic approximations. In this section a set of formulas which can be used to model array coils are collected, and simple methods for minimizing mutual coupling effects are discussed.

Computational methods

Many methods are available to model coils and coils systems. In theory the calculation of mutual impedances and flux densitites of coil arrays over lossy samples is mildly complex. A highly accurate calculation would need to include the inhomogeneities and physical extent of the sample, the current distribution on the coils and their perturbations by the presence of the other coils and the load, and of course the shielding effects on the electric and magnetic fields due to eddy currents introduced in the lossy sample. Several approaches are available that can include some or all of these complications. Examples include analytical solutions for canonical geometries,[8, 48–51] finite element approaches[52–56] integral equation solvers,[57–60] and finite-difference time-domain approaches.[61, 62]

For a great many applications, a simple approach based on quasistatics will provide good results.[6, 17, 19, 27, 63–70] The quasistatic method uses static assumptions to compute the magnetic flux density and the magnetic vector potential, but then assumes a time-varying field to obtain an electric field. The losses in the sample are computed from the electric field. The impedance matrix for the array can then be approximated, as described below. While this is an approximate technique which does not enforce all boundary conditions on the fields, it is considered to be a good approximation for many cases of interest in MRI and MRS. Additionally, the method can be extended to handle multiply connected structures, such as birdcage coils, and even RF shields. An excellent discussion of the basic approach can be found in the text by Smythe.[69] Assuming a known current distribution, the magnetic flux density $\mathbf{B}(\mathbf{r})$ produced by a known current distribution $I(\mathbf{r})$ can be obtained in a straightforward manner from:

$$\mathbf{B}(\mathbf{r})=\frac{\mu}{4\pi}\int_l\frac{I(\mathbf{r}')\mathbf{dl}\times\hat{\mathbf{a}}_R}{R^2} \tag{31}$$

where $\boldsymbol{r}'$ is the vector from the integration point on the conductor to the observation point $\mathbf{r}$, $\mathbf{dl}$ is the differential path length along the conductor at the point of integration. $\hat{\mathbf{a}}_R$ is a unit vector in the direction of $\mathbf{R}=\mathbf{r}-\mathbf{r}'$, the vector from the source to the observation point, with magnitude denoted R. The current distribution $I(\mathbf{r})$ is generally known to a high degree of accuracy for practical, well-performing coils, such as simple loops, planar-pairs, and birdcage designs. Once the current begins to substantially diverge from being constant over a given segment, performance of the coil, as well as this model, begins to suffer.

One can show using the reaction theorem that the port open-circuit impedance parameters can be expressed in terms of the electric fields and currents as:[43]

$$Z_{ij}=\frac{-1}{I_iI_j}\int_v\mathbf{E}^j(\mathbf{r})\cdot\mathbf{J}^i_{coil}(\mathbf{r})dv \tag{32}$$

where $\mathbf{E}^j(\mathbf{r})$ is the electric field due to the assumed constant current distribution on coil j, and $\mathbf{J}^i_{coil}$ is the assumed current distribution on coil i. The vector $\mathbf{r}$ is from the origin to the integration point. I_i and I_j are the port currents for coil i and j. Both the self impedances Z_{ii} and the mutual impedances Z_{ij} are obtained from Eq. (32), which is exact if the current distributions are known and the proper Green's function for the media is used. In this case the actual current on coil i is complex, due to the loss from the coil and the sample. However, one can obtain approximate results by using equivalent sources $\mathbf{J}^i_s(\mathbf{r})$ to account for the lossy medium, characterized by the conductivity $\sigma(\mathbf{r})$. The equivalent sources are the currents induced in the sample by the electric field of coil i,

$$\mathbf{J}_s^i(\mathbf{r}) = \sigma(\mathbf{r})\mathbf{E}^i(\mathbf{r}). \quad (33)$$

We obtain an approximation for the electric fields by ignoring the term due to the divergence of the magnetic vector potential, a quasistatic approximation. This gives the result for the electric field of coil i:

$$\mathbf{E}^i(\mathbf{r}) = -j\omega\mathbf{A}^i(\mathbf{r}) \quad (34)$$

where:

$$\mathbf{A}^i(\mathbf{r}) = \frac{\mu}{4\pi}\int_{coil\,j}\frac{\mathbf{J}^i_{coil}(\mathbf{r}')dv'}{|\mathbf{r}-\mathbf{r}'|} \quad (35)$$

and $\mathbf{r}-\mathbf{r}'$ is the vector from the source point to the observation point. For most coils with a single, simply connected conductor, such as a loop, Eq. (35) becomes:

$$\mathbf{A}^i(\mathbf{r}) = \frac{\mu}{4\pi}\int_{coil\,j}\frac{I^i_{coil}(\mathbf{r}')\mathbf{dl}}{|\mathbf{r}-\mathbf{r}'|} \quad (36)$$

At this point, the integral in Eq. (32) can be expressed in two parts, one forming the reaction of the electric fields of coil j with the equivalent sources representing the lossy sample, and the other the reaction between the fields of coil j and the assumed current on coil i.

$$Z_{ij} = \frac{-1}{I_i I_j}\left\{\int_{sample}\mathbf{E}^j(\mathbf{r})\cdot\mathbf{J}^i_s(\mathbf{r})dv + \int_{\text{coil}}\mathbf{E}^j(\mathbf{r})\cdot\mathbf{J}^i_{coil}(\mathbf{r})dv\right\} \quad (37)$$

Using Eqns (33) and (44), and noting that one can assume an input current in both coils of one amp, leads to approximate expressions for the resistive and reactive coupling terms:

$$R_{ij} = \mathrm{Re}\{Z_{ij}\} \approx \mathrm{Re}\int_{sample} -\mathbf{E}^j(\mathbf{r})\cdot J^i_s(\mathbf{r})dv$$

$$= \sigma\omega^2\int_{sample}\mathbf{A}^j(\mathbf{r})\cdot\mathbf{A}^i(\mathbf{r})dv \quad (38a)$$

$$X_{ij} = \mathrm{Im}\{Z_{ij}\} \approx \mathrm{Im}\int_{coil\,i} -\mathbf{E}^j(\mathbf{r})\cdot J^i_{coil}(\mathbf{r})dv$$

$$= \omega\int_{coil\,i}\mathbf{A}^j(\mathbf{r})\cdot J^i_{coil}(\mathbf{r})dv \quad (38b)$$

Note that the copper loss has been ignored. For coils systems that are not heavily sample loss dominated, one would need to include the copper loss terms, which are widely available. Additionally, any perturbation in the inductive coupling due to the sample is ignored, but this is often a very good approximation.

Figures 3(a) and 3(b) below compares measured results for the mutual impedance between two 4.5 inch o.d. square coils, constructed from 0.5″ copper tape. The coils are 1 and 2 cm from the sample, which is 0.72 S/m conductivity saline. Two sets of calculated results are included, one set computed using the quasistatic approximations above, and the other using a somewhat more complete full-wave approach which uses the proper Green's function for the lossy medium.[71] All data was computed at 63 MHz, where this is a relatively large coil nearly a tenth of a free space wavelength in total conductor length. The current on the square loops was assumed to be constant in both methods. The measured data in these figures were obtained using an HP4195A network analyzer, using methods discussed in the next section. The quasistatic method clearly overestimates the mutual resistance because it does not include the shielding effect of the lossy medium. However, it also overestimates the self resistances of the array elements, which tends to be an offsetting effect. Good agreement is obtained for the mutual reactance, shown in Fig. 3(b). The accuracy will improve at lower conductivities or lower frequencies, but this example demonstrates that the method works reasonably well even for large coils.

Measurement of coil parameters

In most cases the Biot-Savart law, Eq. (31), provides an accurate map of the coil fields. However, if the relative coil positions, or their position with respect to the sample are not known accurately, it may be desirable to map the fields using the spectrometer. It is necessary to provide a phase reference to compensate for phase differences between channels if using a multiple channel receiver. The impedance values can be measured with a network analyzer by measuring the S-parameters and converting to Z-parameters. A network analyzer measures the port relationships in terms of S-parameters, which relate power ratios rather than voltage ratios at the ports.[72] Most network analyzers will automatically convert a single port measurement S_{11} to the self-impedance Z_{11}. The mutual-impedance can be obtained

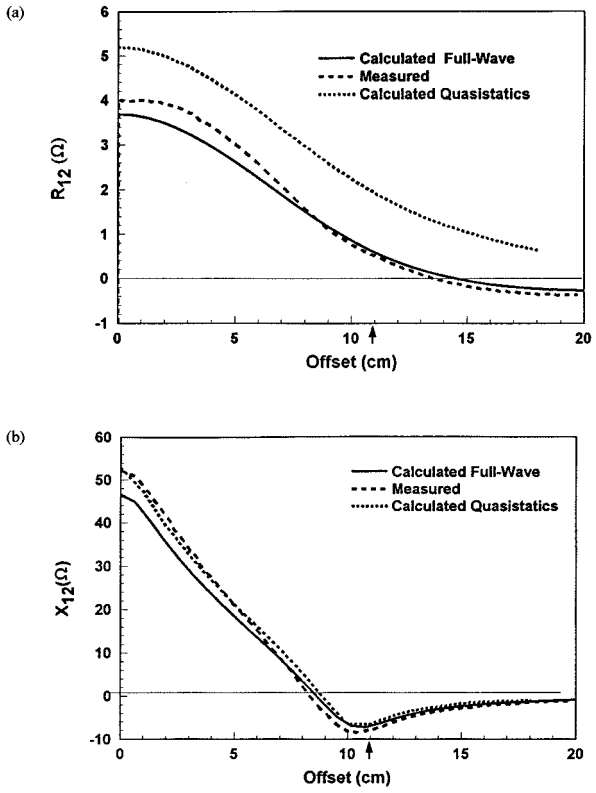

Figure 3. Comparison of measured results to theoretical results for the mutual impedance between two 11.5 cm o.d. square coils constructed from copper tape. The coils are 1 cm and 2 cm from a tank of 0.72 S/m saline solution. Theoretical results are shown from quasistatics and full-wave spectral-domain approaches. In both cases the current distributon on the coils is assumed to be constant. (a) Mutual resistance, and (b) mutual reactance.

by the conversion:

$$Z_{12}=Z_o \frac{S_{12}}{(1-S_{11})(1-S_{22})-S_{12}^2} \tag{39}$$

where Z_o is the characteristic impedance of the measurement network, typically 50 ohms. In the case of a vector impedance meter, one can measure the coil self-impedances directly, and then obtain the mutual impedances from

$$Z_{12}=\sqrt{Z_{22}(Z_{11}-Z_{1,in})}, \tag{40}$$

where $Z_{1,in}$ is the input impedance of the element 1 with the terminals of element 2 short circuited.[45] Using either of these two methods one must be extremely careful to calibrate out the effects of the connectors and/or probes used to connect to the coils in order to obtain accurate results.

Minimization of coil coupling

Coil coupling is determned by two factors, the mutual impedance between two coils, and the relative currents in the coils. The mutual impedance between two coils is defined by Eq. (8), repeated here for convenience:

$$Z_{ij}=\left.\frac{V_i}{I_j}\right|_{I_k=0,\, k\neq j} \tag{41}$$

Z_{ij} is the ratio of the voltage at port i due to an excitation current at port j, with all other ports open-circuited. Note that this includes the effects of the other coils, which, although they are open circuited (I_k=0 in Eq. (41)), may still affect the mutual impedances. For many cases, including simple coils such as circular and rectangular loops, it is a very good approximation to ignore the presence of other open circuited coils when computing mutual impedances. Even though a mutual impedance may exist between coils, Eq. (41) clearly shows that if no current is allowed to flow in coil j, no voltage will be induced in coil i. This indicates two ways to minimize the effects of mutual impedance: reduce the mutual impedance itself, or simply reduce the currents in the coils.

The mutual impedance is a complex quantity consisting of a mutual resistance and a mutual inductance, $Z_{12}=R_{12}+jX_{12}$. The above discussion assumes that the coils have zero mutual inductance, or, alternatively, are operated into an open circuit to eliminate the effects of mutual impedance. If the coils are not operated into open circuits, the currents induced in each coil by the sample magnetization will in turn induce currents in the other coils, significantly complicating the analysis of the array. However, even if the coils are operated into an open-circuit, the presence of mutual resistance can lead to a decrease in the coil efficiency due to an increase in power absorbed in the transmit case, as shown in Eq. (10). An alternative and equivalent viewpoint is that the presence of mutual resistance manifests itself in correlated noise between the channels of the array.

In order to reduce the effects of coupling between coils, we want to: (1) minimize X_{12} by proper coil overlap or cancellation circuitry, (2) minimize noise correlation by proper coil design, using orthogonal modes if possible, and (3) minimize the effects of coupling by using isolation preamplifiers. Each will be briefly discussed.

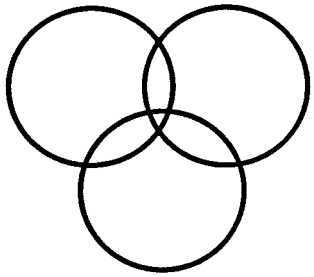

Figure 4. Three round coils overlapped in order to minimize mutual reactance. The necessary overlap is a function of the coil spacing and construction, but is approximately as indicated. This method of minimizing mutual reactance can not be extended beyond three coils.

Mutual inductance cancellation

As mentioned above, the mutual inductance between two simple coils, such as circular or square loops can be driven to zero by proper overlap of the coils, as illustrated in Fig. 4. This is not a complete solution because it cannot in general work for an array with more than three elements, and because the positioning is very sensitive and load dependent. Additionally, the overlap which minimizes mutual inductance is usually not the same as that which minimizes mutual resistance. Because the mutual inductance is the larger of the two coupling mechanisms, it is essential that nearest neighbor coils be overlapped to minimize the mutual inductance. Otherwise, severe coupling will make the two coils operate as one large coil, and the independence between data channels will be lost.

It is also possible to design external circuits which cancel the mutual inductance.[29, 73, 74] For example, Fox has demonstrated such a circuit for a linear spine array.[29]

Orthogonal coils

A somewhat higher standard for geometric decoupling of coils is to use truly orthogonal coils. For these coils, such as a properly aligned planar-pair-loop combination, $Z_{12}=0$. This is the ideal situation, as then there is no need for isolating preamplifiers, the mutual resistance and mutual reactance are zero, and the effects of coupling are eliminated. In terms of noise correlation, since the mutual resistance is zero, or very nearly so, there is negligible noise correlation.

Orthogonal modes are commonly used in quadrature volume coils,[54, 75–79] and are now being used as individual elements in coil arrays. Hyde and his colleagues have suggested a variety of orthogonal mode coils[1, 32, 80, 81] and a variety of others have been suggested, for example ladder network resonantors.[47] One example of a relatively simple coil which can be fed at a number of different ports, is illustrated in Fig. 5.[32] The coil supports three orthogonal modes, excited across different capacitors. All ports are isolated from each other, and hence the signals can be fed into a multiple channel receiver for independent acquisition from each. By combining the signals as discussed above, higher SNR is obtained over what would be obtained from a single coil of the same diameter.

Isolation preamplifiers

Many preamplifiers contain a matching network which transforms the impedance of the amplifier to 50 ohms. The coil is also conjugate matched to 50 ohms, ensuring

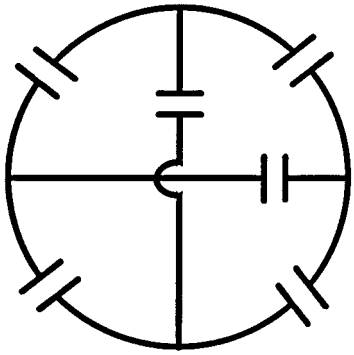

Figure 5. A wheel-and-spoke coil.[32] This coil supports multiple modes whch are in principle, at least, intrinsically isolated. To the extent that the current distributions are constant and there are no significant asymmetries in the sample or coils, the different modes will exhibit zero mutual impedance. Because there is no mutual impedance, no efforts need to be made to minimize the effects of coupling.

maximum power transfer to the preamplifier. A disadvantage of this approach is that significant currents are induced in the coil by the MR signal and the noise sources. If other coils are present and not fully decoupled, these currents will couple to the other coils, degrading SNR.

Alternatively, it is possible to design the preamplifer matching network to present a very high or low impedance at the input while still wanting to 'see' a 50 ohm coil impedance for a noise match. As long as the magnitude of the reflection coefficient of the preamplifier is nearly 1.0, a network can be designed which simultaneously matches the coil to the 50 ohms and transforms the preamplifer impedance to nearly an open circuit, minimizing coil crosstalk. A block diagram of a surface coil with an isolating matching network is shown in Fig. 6. Such a network will minimize the effects of inductive coupling, maintaining the independence of the signals between channels. However, the mutual resistance, which manifests as correlated noise will still be present. This isolation network can be realized in a number of ways. Roemer has suggested a simple network which works well for most standard clinical coils.[6] For coils with low resistance, such as might arise with superconducting coils or coils for microscopy, the networks described in[82] have the additional advantage of allowing the user to vary the network to realize convenient component values. One such network is shown in Fig. 7. For a given coil impedance $Z_L=R_L+jX_L$, the component values for the network in Fig. 7

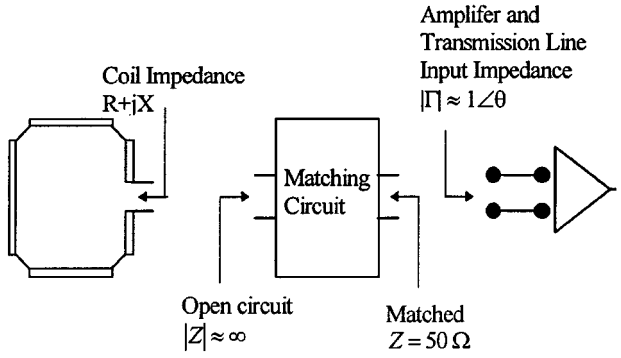

Figure 6. Block diagram illustrating the concept of an isolating matching network. The matching circuit transforms the input impedance of the preamplifier, assumed to be primarily reactive to an open-circuit at the coil input port, significantly reducing the current induced in the coil by the sample, and likewise reducing the effects of mutual coupling. In the other direction, the matching network transforms the impedance of the coil to 50 ohms.

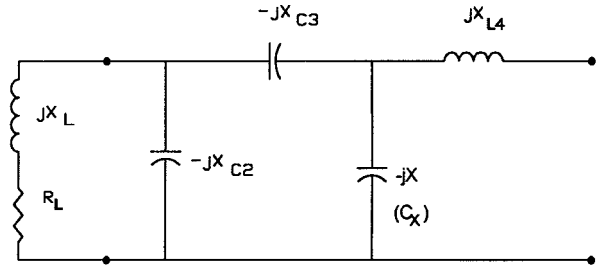

Figure 7. One possible configuration for an isolating matching network. The parameter X can be freely chosen in order to obtain 'good' values for the other components.

are given by Eqn (42a–f). The fourth component, with reactance of X ohms, can be freely chosen.

$$X_{c_2}=\frac{XA}{XZ_o-B} \qquad A=X_LZ_o+R_LX_{Amp}$$

$$X_{c_3}=X\frac{A-B}{B} \qquad B=\sqrt{R_LZ_0(x_{Amp}^2+Z_o^2)} \qquad \text{(42a–f)}$$

$$X_{L_4}=X\frac{A-B}{A}+Z_o\frac{C}{A} \qquad C=R_LZ_o-X_LX_{Amp}$$

EXAMPLES OF PHASED ARRAY COILS FOR NMR SPECTROSCOPY

Several examples are considered to illustrate the advantages as well as the limitations of array coils. The first two examples consider simple planar and volume arrays, followed by several examples of applications of array coils in clinical spectroscopy.

SNR improvements in phased arrays

The first example is a theoretical comparison of a single rectangular surface coil to 2×2, 4×4 and 8×8 arrays of coils which cover the same area as the original single coil. Next, a sixteen element volume coil is compared, both theoretically and experimentally, to a quadrature birdcage coil of the same radius.

An obvious question in designing array coils is what is the proper number and configuration of elements to use. A number of researchers have examined this issue in a variety

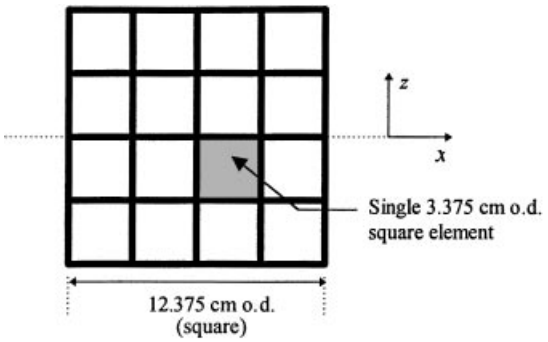

Figure 8. A 16 element array of 3.375×3.375 cm o.d. square elements with 0.375 cm wide copper strip conductors. Elements are overlapped 0.375 cm, and are assumed to be operating into ideal isolating matching networks.

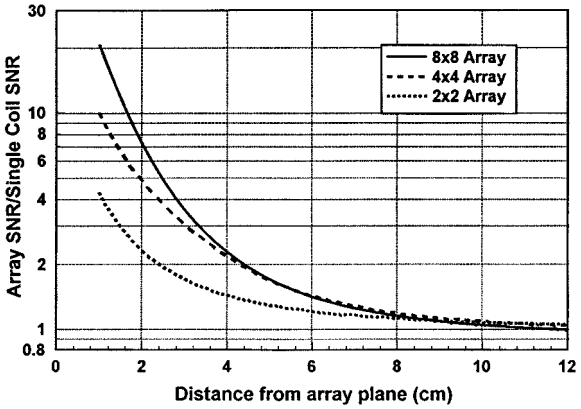

Figure 9. Signal-to-noise ratio (SNR) improvement obtained by using different size coil arrays as compared to a single coil with the same overall dimension. All coils were modeled as being 1 cm over a lossy half-plane consisting of 0.72 S/m saline. SNR data was calculated on a line perpendicular to the coil plane, and over the center of the array.

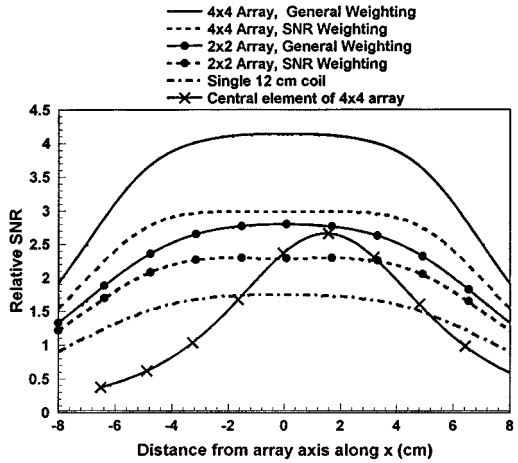

Figure 10. Relative signal-to-noise ratio (SNR) obtained by using different size coil arrays and a single coil with the same overall dimension. All coils were modeled as being 1 cm over a lossy half-plane consisting of 0.72 S/m saline. SNR data was calculated on a line parallel to the coil plane at a height of 4.5 cm over the center of the array, as indicated in Fig. 8.

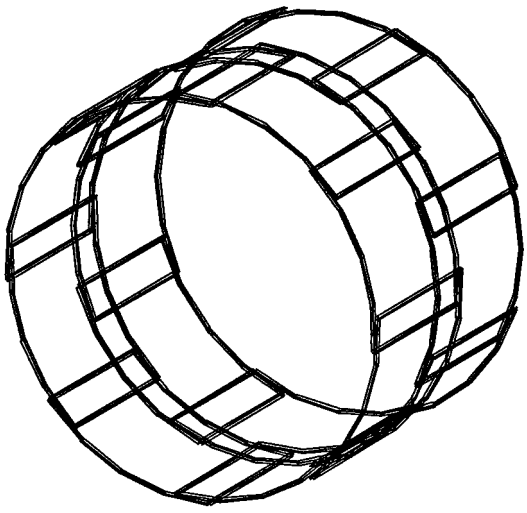

Figure 11. Perspective view of the 16 element head coil array. Array elements consisted of 10.5×12.4 cm rectangular coils made from copper tape placed on the surface of a 26.7 cm o.d. PVC cylinder. The elements were arranged in two rows of eight, overlapped approximately 1 cm.

of clinical applications,[7, 9, 10, 19, 20, 31] but all of these studies were restricted to four coils due to the available hardware. It is interesting to examine the potential benefits of using arrays with a larger number of elements, particularly since initial results have been obtained which consider larger arrays.[8, 72, 83–87] The first example compares the relative SNR of three arrays and a single coil, all with the same overall outer dimension. The single coil has an outer dimension of 12.375 cm in each direction, and is modeled as being constructed from 0.375 cm wide copper tape. Each array was formed from 2×2, 4×4 or 8×8 overlapped coils, overlapped by the width of the copper tape. The 4×4 array is illustrated in Fig. 8. In the case of the 4×4 array, each element is 3.375 cm×3·375 cm in overall dimension. Coils were at $y=0$ in the x–z plane, and the SNR was calculated as a function of y at $x=0$, $z=0$. In order to compute the SNR, the flux density of each coil was computed using the Biot-Savart law as discussed above. The resistance matrix $[R]$ was computed using a full-wave, spectral-domain approach,[88] using a lossy half-plane with $\sigma=0.72$ S/m located 1·0 cm above the coils. The current distribution on each coil was assumed to be uniform, and it was assumed that isolation matching networks were used to eliminate the effects of mutual inductance. In practice one would want to use further means to reduce the effects of mutual inductance, in particular by further overlapping the coils as discussed below. The mutual resistance, included in this

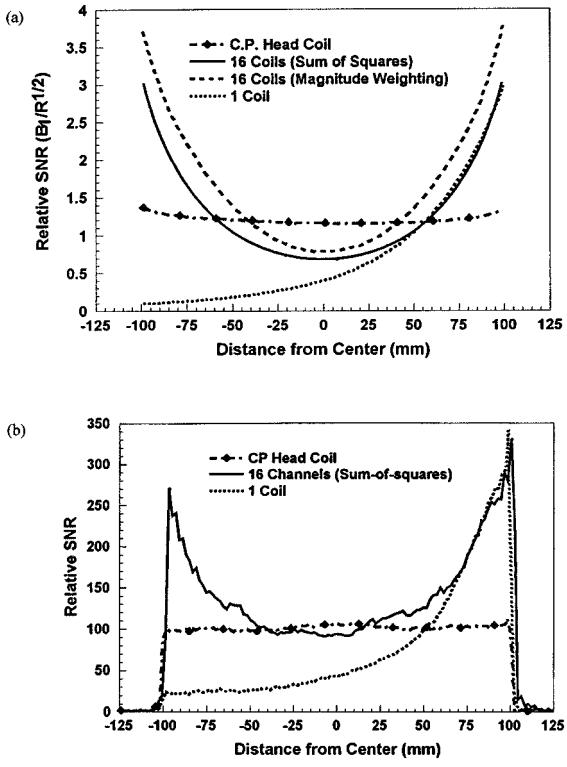

Figure 12. (a) Calculated results comparing the SNR of the 16 channel head coil, a single element in the array, and the standard quadrature head coil. The SNR from the array was calculated for both the most general combination technique and the sum-of-squares method. The array was shorter than the quadrature head coil, resulting in a drop in relative SNR near the center of the array. (b) Measured results comparing the SNR of the 16 channel head coil, a single element in the array, and the standard quadrature head coil. The sum-of-squares method was used to compute the combined data from the array, as the mutual resistance matrix was not measured. Agreement with the theoretical results in (a) are good, demonstrating substantial improvement in SNR near the array elements and comparable performance to the head coil near the center of the array.

model, is a very slow function of coil spacing.

Figure 9 compares the relative SNR on the *y* axis of these three coil arrays to the single element. Several interesting results are demonstrated. Close to the array there is a substantial improvement in SNR obtained by using a greater number of elements. At a distance of 1 cm, the SNR approximately doubles as the number of elements per side is doubled. As one looks further from the array plane, the SNR improvement decreases, until at a distance equal to the diameter of the array the SNR improvement disappears. Importantly, at no point is there a significant degradation of SNR by using the array. The improvement obtained by

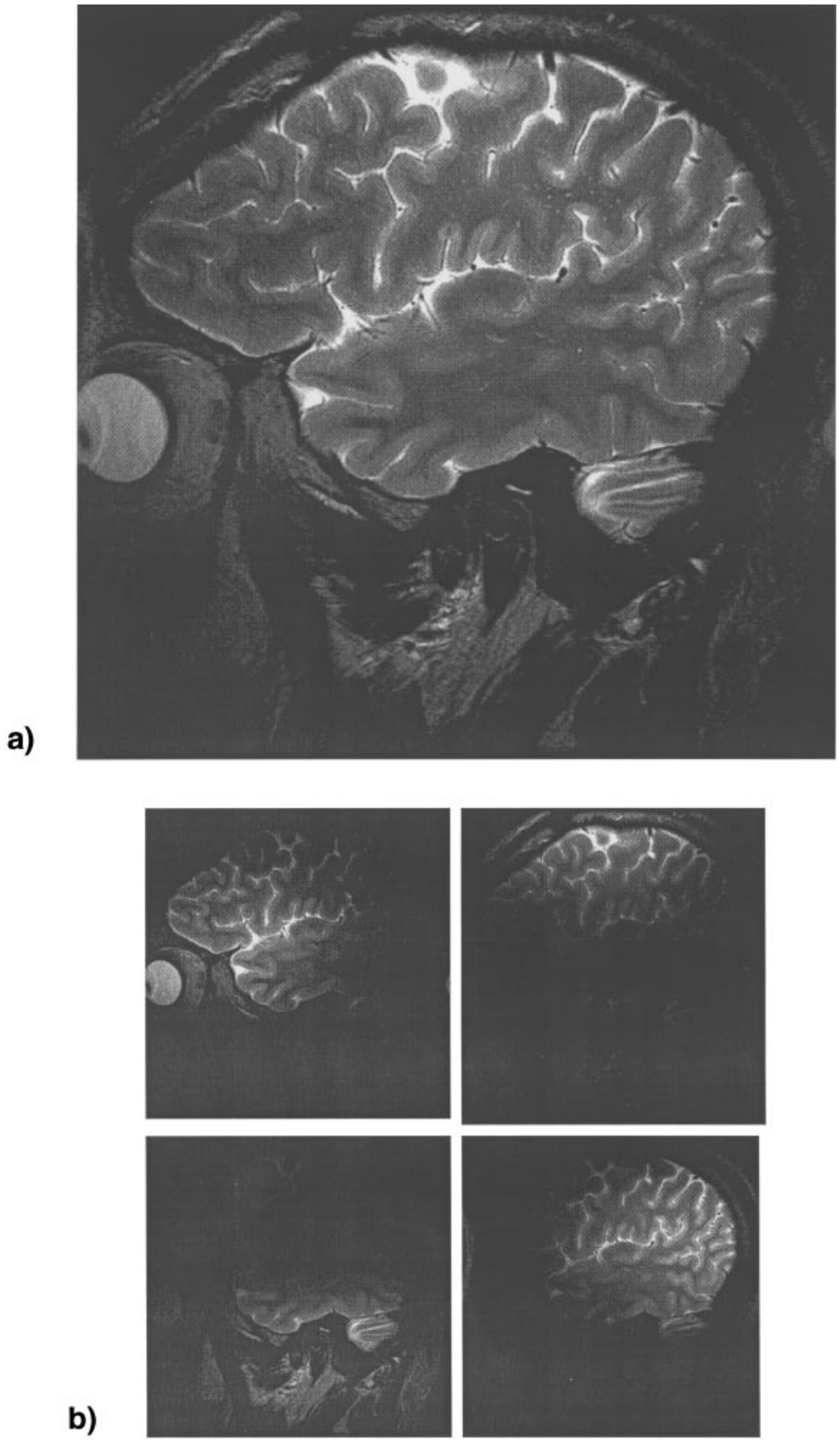

Figure 13. Fast spin echo image of a normal subject acquired with four 8 cm diameter coils arranged in the 'Olympic rings' configuration. 512×384 image matrix, 16 cm field of view, 3 mm slice thickness, total acquisition time=5 min. (a) Image after combination of the data from the four receivers using the sum-of-squares algorithm. (b) Images formed from the individual receivers.

using additional elements is evident, at least for the 16 element array. At a depth of 4 cm the four element array provides over 1.4 times the SNR of a single element with the same overall dimension, while the 16 element array provides better than a factor of 2 improvement. It is interesting that for distances greater than 5 cm the SNR of the 64 element array is actually a bit lower than that of the 16 element array. This is due to the additional copper losses due to the increased number of elements, and illustrates that the most significant benefit of very large arrays is in the region very close to the elements.

The results shown in Fig. 9 were calculated using the SNR weighting technique in Table 1. In this method the noise correlations and relative phases of the coil flux densities are not considered when computing the weighting factors. This information is always available when modeling coils, and can be measured on the spectrometer.[6] Using this additional information one can combine the signals using the most general approach specified in Eqs (22) and (23), yielding substantial improvements in SNR. Figure 10 compares the SNR along the x axis at $y=5$ cm, $z=0$, where the origin is the center of the array. The SNR is shown for the 16 and 4 element arrays, using both general and SNR weighting (equivalent to sum-of-squares in this case). Additionally, the SNR obtained from the single 12.375 cm coil and from a single central 3.375 cm coil from the 16 element array (shown hatched in Fig. 8) are shown. Several conclusions can be drawn. First, the general combination method improves the SNR by nearly a factor of 1.4 in the center of the array, a result that contradicts conclusions by other researchers that no more than an 11% drop in SNR would occur by using the sum-of-squares method.[6] Second, it is interesting to note that the SNR obtained by a single element of the 16 element array is comparable to that obtained from the four element array using general combination, and actually exceeds the SNR obtained using

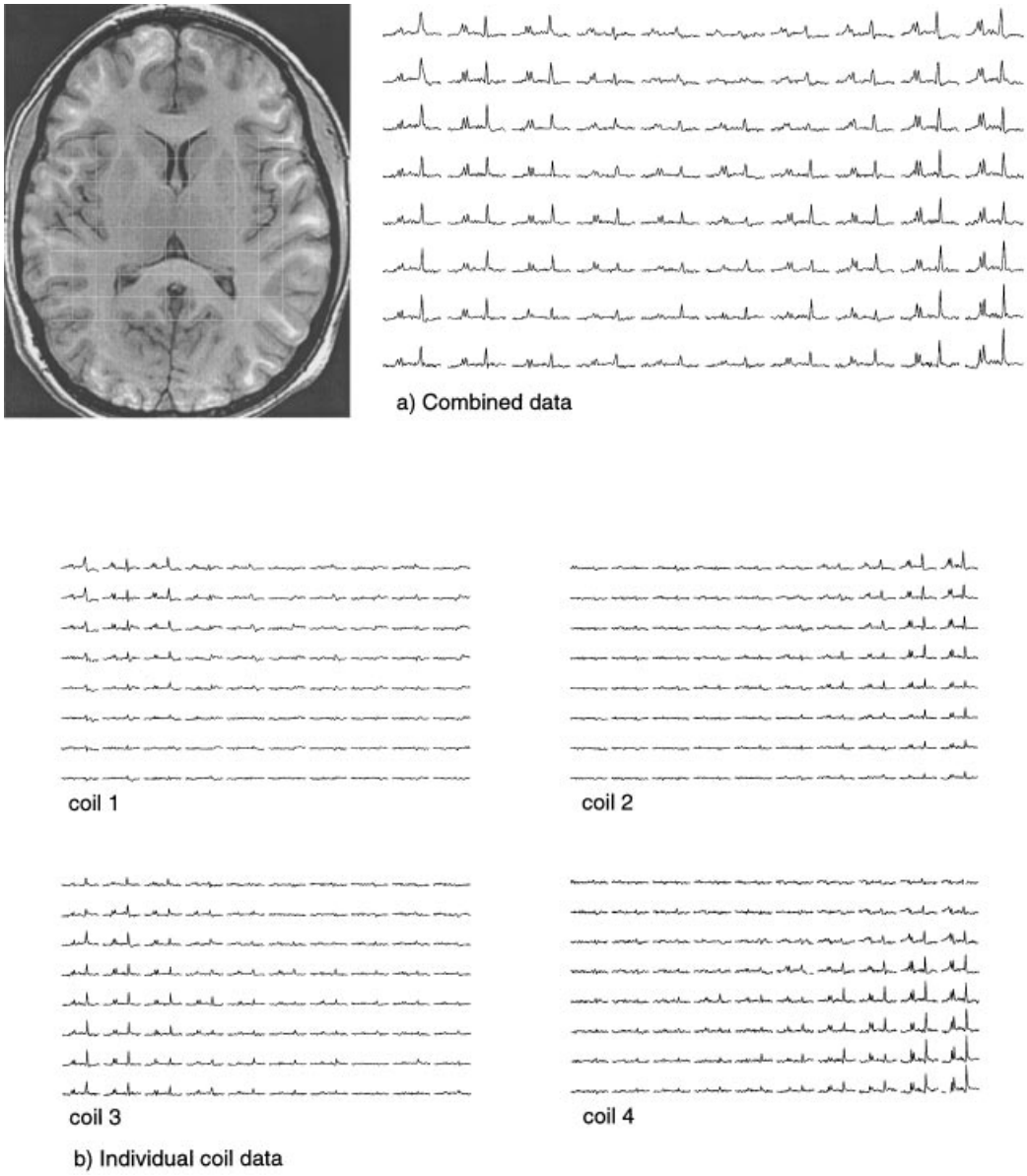

Figure 14. Subset of metabolite spectra from an axial 16 × 16 proton MRSI acquisition obtained with a four coil array of 9 cm diameter coils. Two coils were placed on each side of the head. PRESS localized acquisition, TR/TE = 1500 ms/144 ms, slice thickness = 1 cm, nominal voxel volume = 1 ml, acquisition time = 13 min. (a) Combined data obtained by independently phasing the spectra from each receiver and weighting based on the measured SNR of NAA. Image acquired immediately prior to the MRSI acquisition using the same coil. Image intensity variations have been reduced using a low-pass filter based algorithm. (b) Data from the individual receivers.

sum-of-squares weighting. However, as soon as the point of interest moves from directly over the single coil, the array provides dramatic improvement in SNR.

As a second example, the SNR obtained from a 16 element volume coil array is compared to a standard 1.5 T quadrature head coil (Siemens, Iselin NJ). The array coil consisted of 16 10.5 × 12.4 cm rectangular coils made from copper tape placed on the surface of an 26.7 cm o.d. PVC cylinder, which closely matched the diameter of the birdcage coil used for comparison. The coils were arranged in two rows of 8, and were overlapped approximately 1 cm to minimize inductive coupling. While the array diameter matched the birdcage coil, the length of the array was shorter, at 17.8 cm long. The array element configuration is illustrated in Fig. 11, and further details of the coil construction have been reported elsewhere.[72, 84] SNR comparisons, both theoretical and measured, between the array coil and the standard head coil are shown in Figs 12(a) and 12(b), respectively. Also shown is the SNR of a single element of the 16 channel array. All results were computed with the quasistatic approximations discussed in the previous section. The measured resuts were obtained using a 16 channel time-domain multiplexed MR receiver, installed on a 1.5 T Siemens SP system.[84] The measured and calcuated results agree quite well, both indicating nearly a factor of three improvement in SNR near the array cylinder when using magnitude combination. As in the previous example, the results in Fig. 12(a) indicate that a significant SNR improvement is obtained using a more complete combination algorithm. Third, the SNR near the center of the array is not improved over the original head coil, as one would expect. In fact, as the array is physically shorter than the original head coil, it was expected that the array would have a lower SNR in the center of the field-of-view.

Spectroscopic imaging examples

Some advantages of using array coils for spectroscopic imaging of the brain are illustrated in Figs 13–17.These data were acquired using a 1.5 T General Electric clinical imager capable of phased array imaging from four independent receivers. All of the spectra shown are water-suppressed proton spectra obtained with PRESS localization and two-dimensional (16 × 16) phase encoding.

In Fig. 13, data from a four coil array is combined to give an image with expanded coverage compared to the individual component coils. The images formed from the individual receivers are shown on the right. As prevously

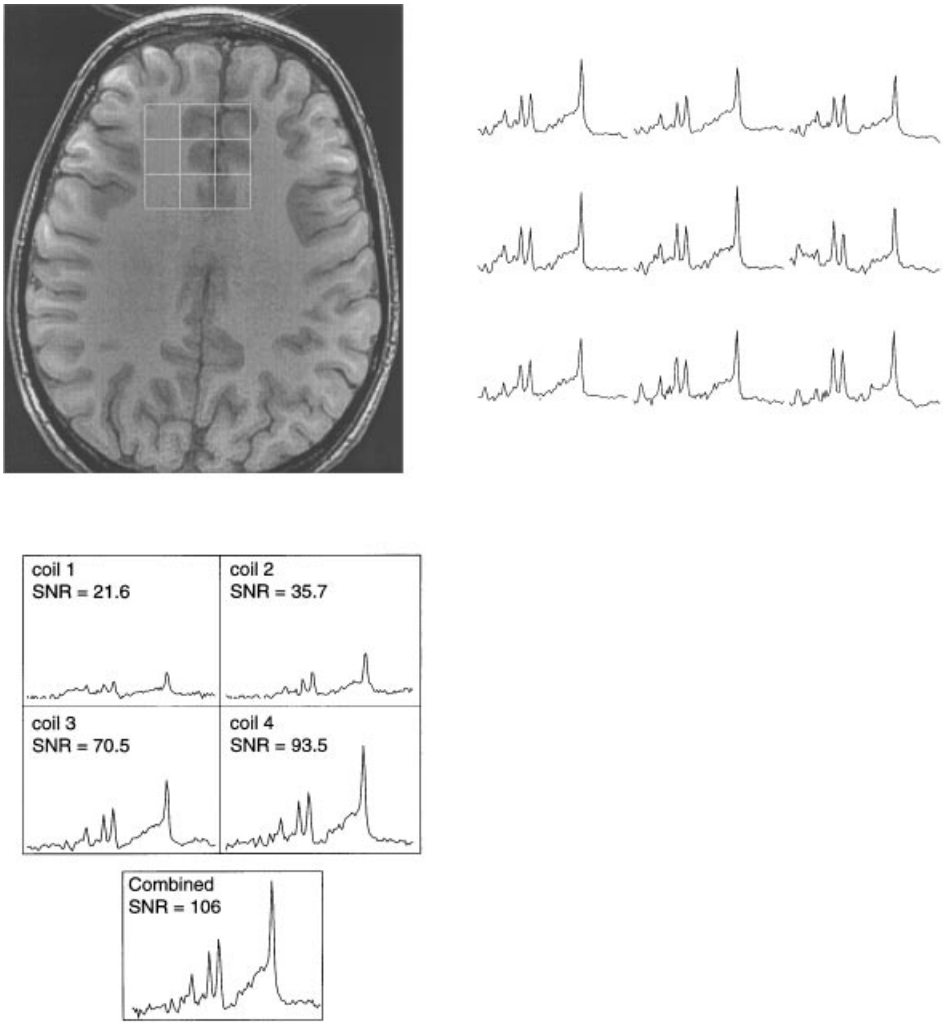

Figure 15. (a) Subset of metabolite spectra in the region of the anterior cingulate cortex from an axial 16 × 16 proton MRSI acquisition obtained with a four coil array of 9 cm diameter coils. Two coils were placed toward the anterior aspect of each side of the head. PRESS localized acquisition, TR/TE = 1500 ms, slice thickness = 15 cm, nominal voxel volume = 2.4 ml, acquisition time = 13 min. (b) The center spectrum from the array shown above illustrating the SNR improvement in the combined spectrum compared to the individual receivers alone.

discussed, the formation of a composite image with maximized SNR requires some knowledge of the SNR of each pixel in the images from the individual receiver is as well as information about the noise correlations between the receivers. The composite image in Fig. 13 was formed using the sum-of-squares algorithm of Eq. (30). In this implementation, the magnitude of the pixel value is used as weighting factor for that pixel. The sum-of-squares method assumes that the intensity of each pixel in the uncombined images is a good approximation of the pixel's SNR for that receiver. This approximation is closest for images with high SNR and the method has been shown to closely approximate the SNR that can be achieved with full knowledge of the complex field maps and resistive coupling matrixes of the coils.[6]

Unfortunately, extending the sum-of-squares method to spectroscopic imaging encounters several problems. (i) The spectral intensity at an arbitrary chemical shift is not necessarily a good approximation of the SNR of the spectrum since most points in the spectra do not contain peaks. (ii) It is desirable to weight every point in the spectrum equally when combining the receivers in order to facilitate comparisons between metabolite levels in a given voxel.

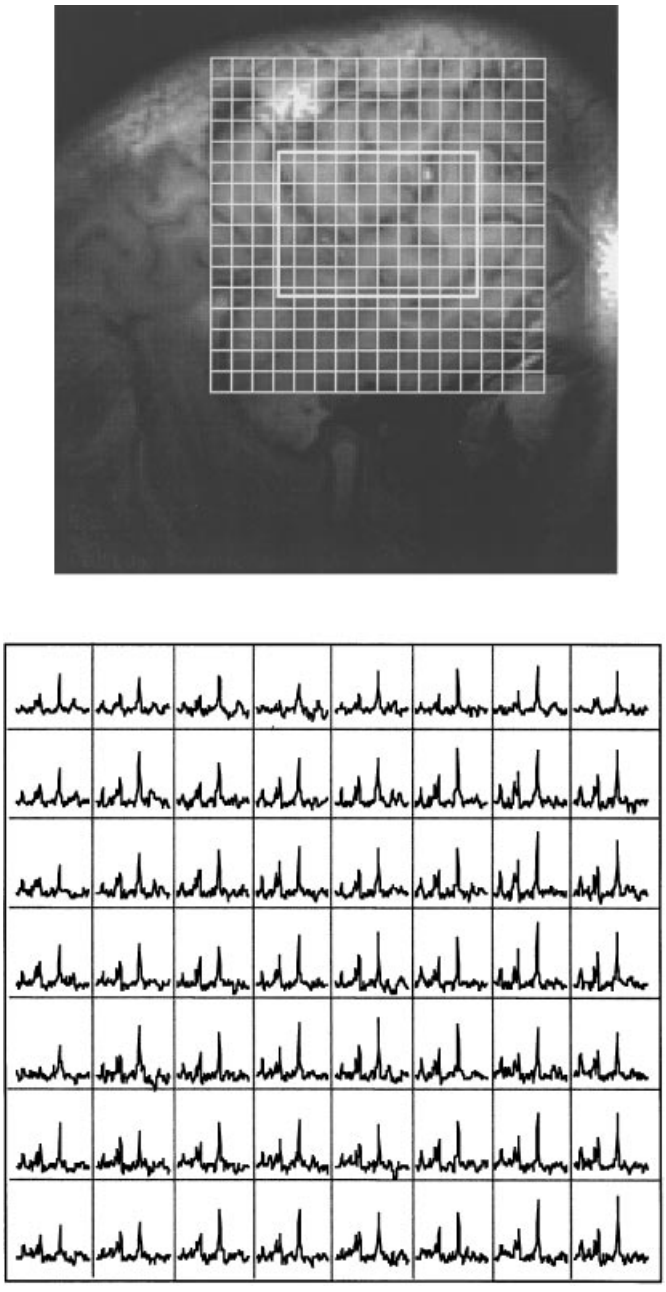

Figure 16. Subset of proton spectra from a high spatial resolution sagittal MRSI acquisition through the superior temporal and parietal lobe. A four coil array of 6 cm diameter coils in the 'Olympic rings' configuration was used. The data shown was combined using the measured SNR of NAA in each voxel. Combination of the data based on a calculated B1 field map of each coil (neglecting coil couplings) showed similar SNR results. PRESS localized acquisition, TR/TE = 1 s/65 ms, slice thickness = 7 cm, nominal voxel volume = 0.18 ml, acquisition time = 17 min.

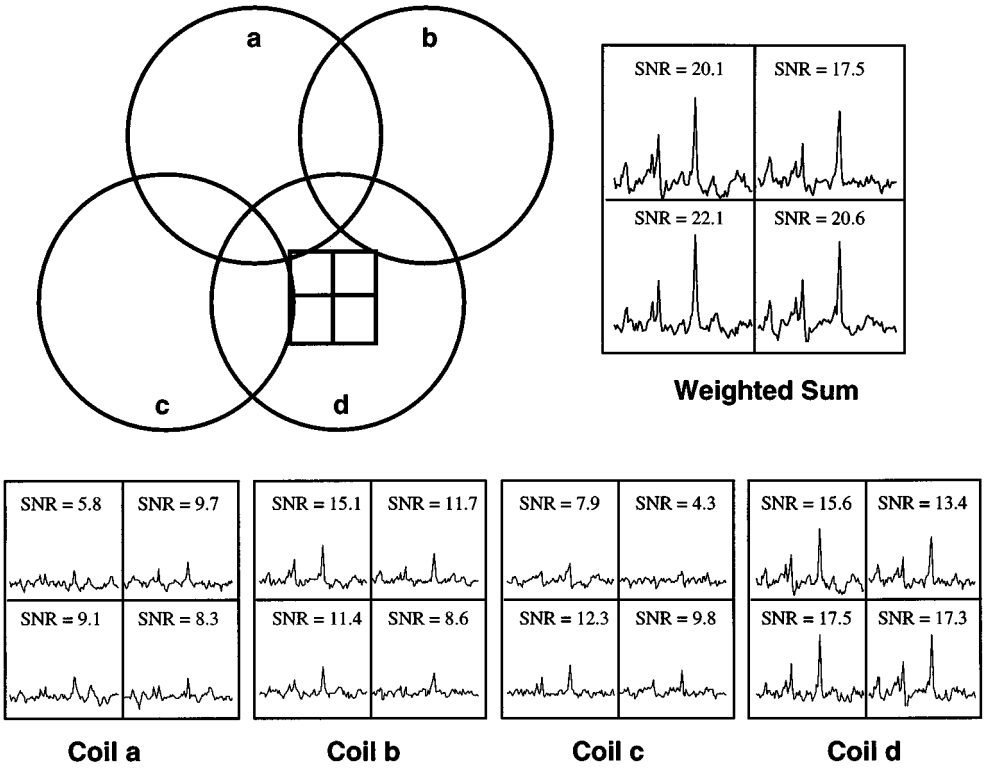

Figure 17. The data from the individual receivers and the weighted sum for four selected voxels from the approximate location indicated. The combined data was formed using SNR weighting based on the NAA peak.

The signal in each spectral voxel can still be estimated in an automated way and used to form the weighting functions, w_{jk}, in Eq. (25). Three possible methods include: (i) The noise and metabolite signal intensity for each voxel can be empirically estimated in the data from each coil. This method, like the sum-of-squares method, has the advantage that all of the information is derived from the data itself; no knowledge of the coil configuration is needed. The signal intensity can be measured from one prominent metabolite peak, as a sum of several peaks, or from the water peak of an unsuppressed reference scan. The latter methods provide robustness for cases when a given metabolite (e.g. NAA) is absent in the subset of the spectra. (ii) A sensitivity map for each coil in the array can also be obtained from low resolution proton density weighted images through the region of interest. The resolution of the image can be further lowered to the resolution of the spectroscopic imaging acquisition by low pass filtering or resampling of *k*-space. (iii) The SNR map for each coil and/or the noise resistance matrix can be computed from the geometry of the coils using Eq. (31).

All of these methods assume that the detection efficiency of the coils in the array does not vary significantly over the spectroscopic voxel; namely, the spatial localization is dominated by the spectroscopic imaging, PRESS or STEAM localization parameters and not the surface coil detection sensitivity profile. A significant variation in the coil detection efficiency over the spectral voxel will produce two problems for the phased array combination techniques outlined above. (a) A large spectroscopic voxel with heterogeneous tissue types might cause the different receivers to record spectra with different metabolite ratios. This case might arise if two small coils are used to detect the spectrum from a large voxel or unlocalized region containing abnormal tissue at one end and normal tissue at the other. (b) The coefficient used to weight the spectra from a given receiver will be only single number used to approximate the range of SNRs present over the volume of the voxel. For example, the SNR in the combined spectrum will be less than optimum if the weight value is derived from an average of the coil SNR map over the voxel and the spectra was dominated by tissue in one end of the voxel.

Figure 14 shows the individual receiver and combined data for PRESS localized $16\times16\times1$ axial spectroscopic image of a normal subject. The data from the individual receivers were combined using the SNR of NAA as the weighting factor and the 'noise normalized' scale constant of Eq. (23). The spectra were independently phased prior to combination. Comparing the data from the individual receivers with the combined data demonstrates the extended coverage of the array compared with any of the individual elements.

Figures 15–17 show the combined data and selected spectra from the individual receivers for a bilateral and unilateral four element array. The increased sensitivity afforded by the small coils of the array was used in Fig. 15 to provide high SNR spectra at modest spatial resolution for the analysis of the glutamate+glutamine levels in the anterior cingulate region. In addition to reducing the signal reception inhomogeneities that would occur using a single small coil, combination of the data from the multiple receivers provided an ~10% increase in SNR over the single receiver with the highest sensitivity. In Fig. 16, a unilateral array of four coils was used to achieve high spatial resolution spectra (nominal voxel volume = 0.2 ml) in the cortex. In both acquisitions the combined data showed an increase in SNR compared to the individual receiver data for all the spectra in the PRESS localized region.

DISCUSSION

The choice of a reception coil for spectroscopic imaging requires evaluating numerous trade-offs between the benefits and liabilities of the various possible choices of volume coils, single element surface coils and array coils. Within these limitations, the array coil can provide both extended capabilities and increased flexibility compared with conventional volume and surface coils.

As illustrated in Fig. 9, improved sensitivity at all depths can be achieved by replacing a single coil with an array of multiple smaller coils covering the same area. The largest benefit is obtained at depths closer to the array, but the marginal increase at greater depths suggests that it is not necessary to sacrifice sensitivity at points distant from the array to gain sensitivity near the coils. For example, Hardy *et al.* used the improved sensitivity profile of a four coil array to improve the spatial resolution of 31P cardiac spectroscopy.[25] Further work by this group has analyzed the sensitivity of various array designs at multiple locations in the heart.[83]

A second problem that can be addressed with array coils occurs when the anatomy of interest lies at a constant depth but extends over a larger region than could be imaged with a single surface coil optimized for that depth. Multiple non-interacting receivers allow these two parameters (sensitivity at a given depth and area of coverage) to be approached more indepedently by optimizing the size of the individual coils to give optimum sensitivity at the depth of interest and increasing the number of coils to cover the required area. Spine imaging is an example of this type of application and was demonstrated by Roemer.[6] Other examples include imaging of the temporomandibular joints,[1] hippocampus[89] and brain cortex.[89] The latter studies also illustrate the advantage of being able to use surface coil arrays to simultaneously image both sides of the body.

The initial studies indicate significant potential for the use of array coils in MRS, and particularly in CSI. Just as in MRI applications, the optimal configuration of the array coil needs to be evaluated for each application. At present, the user is limited to four coils, but the number of available channels may increase in the future, increasing the need for further studies of array coil optimization. Similarly, the existing studies have used simple SNR weighting or the sum-of-squares method. Results presented here and elsewhere[36] indicate that there may be significant improvement obtained by using the more general combination techniques, which require information about the resistance or noise-correlation matrix and the field maps. Currently this information requires additional time and processing to obtain, but in the future the ability to obtain this information could certainly be included in the system software.

Acknowledgements

The authors gratefully acknowledge the contribution of Daniel Vigneron and his group at the Magnetic Resonance Science Center, University of California at San Francisco. The coils and experiments of Fig. 13, 16 and 17 were developed at UCSF. The assistance of Jay Porter and Arne Reykowski in the construction of the sixteen channel head coil and the SNR measurements is also gratefully acknowledged. This work was partially supported by the National Science Foundation grant BCS-9308921, the Whitaker Foundation, and Siemens Medical Systems.

REFERENCES

1. Hyde, J. S., Jesmanowicz, A., Froncisz, W., Kneeland, J. B. and Grist, T. M. Parallel image acquisition for noninteracting local coils. *J. Magn. Reson.* **70**, 512–517 (1987).
2. Boskamp, E. B. A new revolution in surface coil technology: the array surface coil. *Proceedings of the 6th Annual Meeting of the Society of Magnetic Resonance in Medicine.* Abstr., p. 405 (1987).
3. Requardt, H. and Tyrell, R. Switched array coils: a new multi-purpose tool in MRI. *Proceedings of the 6th Annual Meeting of the Society of Magnetic Resonance in Medicine.* Abstr., p. 408 (1987).
4. Wright, S. M., Magin, R. L. and Kelton, J. R. Arrays of mutually coupled local coils for high resolution MR imaging. *Procedings of the 6th Annual Meeting of the Society of Magnetic Resonance in Medicine.* Abstr., p. 96 (1987).
5. Edelstein, W. A., Glover, G. H., Hardy, C. J. and Redington, R. W. The intrinsic signal-to-noise ratio in NMR imaging. *Magn. Reson. Med.* **3**, 604–618 (1986).
6. Roemer, P. B., Edelstein, W. A., Hayes, C. E., Souza, S. P. and Mueller, O. M. The NMR phased array. *Magn. Reson. Med.* **16**, 192–225 (1990).
7. Wald, L. L., Carvajal, L., Moyher, S. E., Nelson, S. J., Grant, P. E., Barkovich, A. J. and Vigneron, D. B. Phased array detectors and an automated intensity-correction algorithm for high-resolution mr imaging of the human brain. *Magn. Reson. Med.* **34**, 433–439 (1995).
8. Wang, J., Reykowski, A. and Dickas J. Calculation of the signal-to-noise ratio for simple surface coils and arrays of coils. *IEEE Trans. Biomed. Eng.* **42**, 908–917 (1995).
9. Hayes, C. E., Mathis, C. M. and Yuan, C. Surface coil phased arrays for high-resolution imaging of the carotid arteries. *J. Magn. Reson. Imaging* **6**, 109–112 (1996).
10. Wald, L. L., Moyher, S. E., Day, M. R., Nelson, S. J. and Vigneron, D. B. Proton spectroscopic imaging of the human brain using phased array detectors. *Magn. Reson. Med.* **34**, 440–445 (1995).
11. Fayad, Z. A., Connick, T. J. and Axel, L. An improved quadrature or phased-array coil for MR cardiac imaging. *Magn. Reson. Med.* **34**, 186–193 (1995).
12. Sinha, S., Gorczyca, D. P., De Bruhl, N. D., Shellock, F. G., Gausche, V. R. and Bassett, L. W. MR imaging of silicone breast implants: comparison of different coil arrays. *Radiology* **187**, 284–286 (1993).
13. Alley, M. T., Grist, T. M. and Swan, J. S. Development of a phased-array coil for the lower extremities. *Magn. Reson. Med.* **34**, 260–267 (1995).
14. Monroe, J. W., Schmalbrock, P. and Spigos, D. G. Phased array coils for upper extremity MRA. *Magn. Reson. Med.* **33**, 224–229 (1995).
15. Kojima, K. Y., Szumowski, J., Sheley, R. C. and Quinn, S. F. Lower extremities: MR angiography with a unilateral telescopic phased-array coil. *Radiology* **196**, 871–875 (1995).
16. Swan, J. S., Grist, T. M., Weber, D. M., Sproat, I. A. and Wojtowycz, M. M. MR angiography of the pelvis with variable velocity encoding and a phased-array coil. *Radiology* **190**, 363–369 (1994).
17. Famili, N., Wright, S. M. and Porter, J. R. MR flow measurement using RF phase gradients in receiver coil arrays. *IEEE Trans. Biomed. Eng.* **40**, 1243–1249 (1993).
18. Strauss, W. L., Tsuruda, J. S. and Richards, T. L. Partial volume effects in volume-localized phased-array proton spectroscopy of the temporal lobe. *J. Magn. Reson. Imaging* **5**, 433–436 (1995).
19. Constantinides, C. D., Westgate, C. R., O'Dell, W. G., Zerhouni, E. A. and McVeigh, E. R. A phased array coil for human cardiac imaging. *Magn. Reson. Med.* **34**, 92–98 (1995).
20. Schmalbrock, P., Pruski, J., Sun, L., Rao, A. and Monroe, J. W. Phased array RF coils for high-resolution MRI of the inner ear and brain stem. *J. Comput. Assist. Tomogr.* **19**,

8–14 (1995).
21. Bernstein, M. A., Grgic, M., Brosnan, T. J. and Pelc, N. J. Reconstructions of phase contrast, phased array multicoil data. *Magn. Reson. Med.* **32**, 330–334 (1994).
22. Yuan, C., Murakami, J. W., Hayes, C. E., Tsuruda, J. S., Hatsukami, T. S., Wildy, K. S., Ferguson, M. S. and Strandness, D. E. Jr. Phased-array magnetic resonance imaging of the carotid artery bifurcation: preliminary results in healthy volunteers and a patient with atherosclerotic disease. *J. Magn. Reson. Imaging* **5**, 561–565 (1995).
23. Breslau, J. Dalley, R. W., Tsuruda, J. S., Hayes, C. E. and Maravilla, K. R. Phased-array surface coil MR of the orbits and optic nerves. *AJNR Am. J. Neuroradiol.* **16**, 1247–1251 (1995).
24. Foo, T. K., Macfall, J. R., Sostman, H. D. and Hayes, C. E. Single-breath-hold venous or arterial flow-suppressed pulmonary vascular mr imaging with phased-array coils. *J. Magn. Reson. Imaging* **3**, 611–616 (1993).
25. Hardy, C. J., Bottomley, P. A., Rohling, K. W. and Roemer, P. B. An NMR phased array for human cardiac 31P spectroscopy. *Magn. Reson. Med.* **28**, 54–64 (1992).
26. Schnall, M. D., Connick, T., Hayes, C. E., Lenkinski, R. E. and Kressel, H. Y. MR imaging of the pelvis with an endorectal-external multicoil array. *J. Magn. Reson. Imaging* **2**, 229–232 (1992).
27. Wright, S. M., Magin, R. L. and Kelton, J. R. Arrays of mutually coupled receiver coils: theory and application. *Magn. Reson. Med.* **17**, 252–268 (1991).
28. Holland, G. N., Blakeley, D. M. and Burke, D. W. Simultaneous imaging with multiple coils using digital transmit and receive coils. *Proceedings of the 9th Annual Meeting of the Society of Magnetic Resonance in Medicine.* Abstr., p. 1143 (1990).
29. Fox, T. R. Capative network to cancel coupling between channels in MRI quadrature antennas. *Proceedings of the 8th Annual Meeting of the Society of Magnetic Resonance in Medicine.* Abstr., p. 99 (1989).
30. Murakami, J. W., Hayes, C. E. and Weinberger, E. Intensity correction of phased-array surface coil images. *Magn. Reson. Med.* **35**, 585–590 (1996).
31. Hayes C. E., Dietz, M. J., King, B. F. and Ehman, R. L. Pelvic imaging with phased-array coils: quantitative assessment of signal-to-noise ratio improvement. *J. Magn. Reson. Imag.* **2**, 321–326 (1992).
32. Tan, G., Song, W., Jesmanowicz, A. *et al.* Multi-channel magnetic resonance spectroscopy. *Proceedings of the 12th Annual Meeting of the Society of Magnetic Resonance in Medicine.* Abstr., p. 370 (1993).
33. Nicklaus, D. J. Use of multiple receive coils for improved signal-to-noise in large field-of-view chemical shift imaging. *Proceedings of the 9th Annual Meeting of the Society of Magnetic Resonance in Medicine.* Abstr., p. 1142 (1990).
34. Redpath,T. W. Noise correlation in multicoil receiver systems. *Magn. Reson. Med.* **24**, 85–89 (1992).
35. Duensing, G. R., Brooker, H. R. and Fitzsimmons, J. R. Maximizing signal-to-noise ratio in the presence of coil coupling. *J. Magn. Reson. B.* **111**, 230–235 (1996).
36. Hayes, C. E. and Roemer, P. B. Noise correlations in data simultaneously acquired from multiple surface coil arrays. *Magn. Reson. Med.* **16**, 181–191 (1990).
37. Jesmanowicz, A., Hyde, J. S., Froncisz, W. and Kneeland, J. B. Noise correlation. *Magn. Reson. Med.* **20**, 36–47 (1991).
38. Jesmanowicz, A. and Hyde, J. S. Noise correlation exists for independent RF coils [letter]. *Magn. Reson. Med.* **25**, 408 (1992).
39. Harpen, M. D. Noise correlations exists for independent RF coils. *Magn. Reson. Med.* **23**, 394–397 (1992).
40. Porter, J. R., Wright, S. M. and Famili, N. A four-channel time domain multiplexer: a cost-effective alternative to multiple receivers. *Magn. Reson. Med.* **32**, 499–504 (1994).
41. Wright, S. M. and Porter, J. R. Parallel acquisition of MR images using time multiplexed coils. *Electronic Letters* **28**, 71–72 (1992).
42. Varosi, S. M., Duensing, G. R. and Fitzsimmons, J. R. Multiplexing applied to a digital MR receiver. *Proceedings of the 3rd Annual Meeting of the Society of Magnetic Resonance.* Abstr., p. 1009 (1995).
43. Harrington, R. F. *Time-Harmonic Electromagnetic Fields*. McGraw-Hill, New York (1961).
44. Hoult, D. I. and Lauterbur, P. C. The sensitivity of the zeugmatographic experiment involving human samples. *J. Magn. Reson.* **34**, 425–433 (1979).
45. Stutzman, W. L. and Theile, G. *A. Antenna Theory and Design.* John Wiley and Sons, New York (1981).
46. Lo, Y. T., Lee, S. W. and Lee, Q. H. Optimization of directivity and signal-to-noise ratio of an arbitrary antenna array. *Proc. IEEE* **54**, 1033–1045 (1966).
47. Ballon, D. and Meyer, K. L. Two-dimensional ladder network resonators. *J. Magn. Reson., A* **111**, 23–28 (1994).
48. Roschmann, P. Radiofrequency penetration and absorption in the human body: limitations to high-field whole-body nuclear magnetic resonance imaging. *Med. Phys.* **14**, 922–931 (1987).
49. Foo, T. K., Hayes, C. E. and Kang, Y. W. An analytical model for the design of rf resonators for mr body imaging. *Magn. Reson. Med.* **21**, 165–177 (1991).
50. Harpen, M. D. Eddy current distributions in cylindrical samples: effect on equivalent sample resistance. *Phys. Med. Biol.* **34**, 1229–1238 (1989).
51. Harpen, M. D. Influence of skin depth on nmr coil impedance. *Phys. Med. Biol.* **33**, 329–337 (1988).
52. Simunic, D., Wach, P., Renhart, W. and Stollberger, R. Spatial distribution of high-frequency electromagnetic energy in human head during mri: numerical results and measurements. *IEEE Trans. Biomed. Eng.* **43**, 88–94 (1996).
53. Li, S., Yang, Q. X. and Smith, M. B. RF coil optimization: evaluation of B1 field homogeneity using field histograms and finite element calculations. *Magn. Reson. Imag.* **12**, 1079–1087 (1994).
54. Vaughan, J. T., Hetherington, H. P., Otu, J. O., Pan, J. W. and Pohost, G. M. High frequency volume coils for clinical NMR imaging and spectroscopy. *Magn. Reson. Med.* **32**, 206–218 (1994).
55. Harrison, J. H. and Vaughan, J. T. Finite element modeling of head coils for high-frequency magnetic resonance imaging applications. *12th Annual Review of Progress in Applied Computational Electromagnetics*, Abst., p. 1220–1226 (1996).
56. Jin, J. M. *The Finite Element Method in Electromagnetics*. Wiley, New York (1993).
57. Harrington R. F. *Field Computation by Moment Methods.* Krieger, Malabar, FL (1982).
58. Wright, S. M. FFT calculation of RF coil coupling surfaces. *Proceedings of the 12th Annual Meeting of the Society of Magnetic Resonance in Medicine.* Abstr., p. 1325 (1993).
59. Ochi, H., Yamamoto, E., Sawaya, K. *et al.* Calculation of electromagnetic fields of an MRI antenna loaded by a body. *Proceedings of the 12th Annual Meeting of the Society of Magnetic Resonance in Medicine.* Abstr., p. 4021 (1992).
60. Wust, P., Nadobny, J., Seebass, M., Dohlus, J. M., John, W. and Felix, R. 3-D computation of E fields by the volume-surface integral equation (VSIE) method in comparison with the finite-integration theory (FIT) method. *IEEE Trans. Biomed. Eng.* **40**, 745–759 (1993).
61. Gandhi, O. P., Gao, B. Q. and Chen, J. Y. A frequency-dependent finite-difference time-domain formulation for induced current calculations in human beings. *Bioelectromagnetics* **13**, 543–555 (1992).
62. Han, Y. and Wright, S. M. Analysis of RF penetration effects in MRI using finite-difference time-domain method. *Proceedings of the 12th Annual Meeting of the Society of Magnetic Resonance in Medicine.* Abstr., p. 1327 (1993).
63. Pascone, R., Vullo, T., Farrelly, J. and Cahill, P. T. Explicit treatment of mutual inductance in eight-column birdcage resonators. *Magn. Reson. Imag.* **10**, 401–401 (1992).
64. Pascone, R. J., Garcia, B. J., Fitzgerald, T. M., Vullo, T., Zipagan, R. and Cahill, P. T. Generalized electrical analysis of low-pass and high-pass birdcage resonators. *Magn. Reson. Imag.* **9**, 395–408 (1991).
65. Vullo, T., Pascone, R., Mancuso, R. and Cahill, P. T. Transmission line analysis of noncylindrical birdcage resonators. *Magn. Reson. Imag.* **12**, 785–797 (1994).
66. Pascone, R., Vullo, T., Farrelly, J., Mancuso, R. and Cahill, P. T. Use of transmission line analysis for multi-tuning of birdcage resonators. *Magn. Reson. Imag.* **11**, 705–715 (1993).
67. Wright, S. M. and Porter, J. R. An enhanced Biot-Savart law modeling technique for RF coils with unknown current distributions and shields. *Proceedings of the 2nd Annual*

Meeting of the Society of Magnetic Resonance. Abstr., p. 1131 (1994).
68. Lawry, T. J., Weiner, M. W. and Matson, G. B. Computer modeling of surface coil sensitivity. *Magn. Reson. Med.* **16**, 294–302 (1990).
69. Smythe, W. R. *Static and Dynamic Electricity,* 3rd edn. McGraw-Hill, New York (1968).
70. Jin, J., Shen, G. and Perkins, T. On the field inhomogeneity of a birdcage coil. *Magn. Reson. Med.* **32**, 418–422 (1994).
71. Wright, S. M., Porter, J. R., Boyer, J. *et al.* Characterization of coupling in planar array coils with arbitrary element geometries. *Proceedings of the IEEE Engineering, Medicine and Biological Society 16th Meeting.* Abstr. (1994).
72. Wright, S. M., Porter, J. R. Reykowski, A. *et al.* A 16 channel time-multiplexed head coil array for functional MR imaging. *Proceedings of the IEEE Engineering, Medicines and Biological Society 17th Meeting.* Abstr., p. 473–474 (1995).
73. Wang, J. A novel method to reduce the signal coupling of surface coil for MRI. *Proceedings of the 4th Annual Meeting of the Society of Magnetic Resonance.* Abstr., p. 1434 (1996).
74. Reykowski, A. Theory and design of synthesis array coils for magnetic resonance imaging. Ph.D. Dissertation. Texas A&M University (1997).
75. Fitzsimmons, J. R., Beck, B. L. and Brooker, H. R. Double resonant quadrature birdcage. *Magn. Reson. Med.* **30**, 107–114 (1993).
76. Hoult, D. I., Chen, C. N. and Sank, V. J. Quadrature detection in the laboratory frame. *Magn. Reson. Med.* **1**, 339–353 (1984).
77. Wong, E. C., Tan, G. and Hyde, J. S. A quadrature transmit-receive endcapped birdcage coil for imaging of the human head at 125 MHz. *Proceedings of the 12th Annual Meeting of the Society of Magnetic Resonance in Medicine.* Abstr., p. 1344 (1993).
78. Beck, B. L., Duensing, G. R., Fitzsimmons, J. R. *et al.* Linear and quadrature characteristics of an elliptical birdcage. *Proceedings of the 2nd Annual Meeting of the Society of Magnetic Resonance.* Abstr., p. 1111 (1994).
79. Murphy-Boesch, J. Srinivasan, R., Carvajal, L. and Brown, T. R. Two configurations of the four-ring birdcage coil for 1H imaging and 1H-decoupled 31P spectroscopy of the human head. *J. Magn. Reson. B.* **103**, 103–114 (1994).
80. Hyde, J. S., Jesmanowicz, A., Grist, T. M., Froncisz, W. and Kneeland, J. B. Quadrature detection surface coil. *Magn. Reson. Med.* **4**, 179–184 (1987).
81. Song, W., Jesmanowicz, A. and Hyde, J. S. A wheel and spoke multi-mode receiver coil. *Proceedings of the 12th Annual Meeting of the Society of Magnetic Resonance in Medicine.* Abstr., p. 1334 (1993).
82. Reykowski, A., Wright, S. M. and Porter, J. R. Design of matching networks for low noise preamplifiers. *Magn. Reson. Med.* **33**, 848–852 (1995).
83. Bottomley, P. A., Olivieri, C. H. L. and Giaquinto, R. What is the optimum phased array coil design for cardiac and torso magnetic resonance? *Magn. Reson. Med.* **37**, 591 (1997).
84. Porter, J. R. and Wright, S. M. A hybrid sixteen channel multiplexed MRI receiver. *Proceedings of the 3th Annual Meeting of the Society of Magnetic Resonance.* Abstr., p. 978 (1995).
85. Kwiat, D., Einav, S. and Navon, G. A decoupled coil, detector array for fast image acquisition in magnetic resonance imaging. *Med. Phys.* **18**, 251–265 (1991).
86. Leussler, C. A flexible 6 element synergy neck coil. *Proceedings of the 3rd Annual Meeting of the Society of Magnetic Resonance.* Abstr., p. 79 (1995).
87. Vesselle, H. and Collin, R. E. The signal-to-noise ratio of nuclear magnetic resonance surface coils and application to a lossy dielectric cylinder model, Part II: the case of cylindrical window coils. *IEEE Trans. Biomed. Eng.* **42**, 507–520 (1995).
88. Wright, S. M. Analysis of electrically small resonator arrays for magnetic resonance imaging using the FFT and conjugate gradient method. *Proceedings of Progress in Electromagnetics Research (PIERS)*, Abstr., p. 739 (1993).
89. Hayes, C. E., Tsuruda, J. S. and Mathis, C. M. Temporal lobes: surface MR coil phased-array imaging. *Radiology* **189**, 918–920 (1993).

